5908 *Biochemistry* **2009,** *48,* 5908–5921
DOI: 10.1021/bi900300r

BIOCHEMISTRY
including biophysical chemistry & molecular biology
Article

Structural Insights into the Calmodulin−Munc13 Interaction Obtained by Cross-Linking and Mass Spectrometry

Kalina Dimova,[‡,§] Stefan Kalkhof,[∥] Ines Pottratz,[∥] Christian Ihling,[∥] Fernando Rodriguez-Castaneda,[⊥] Thomas Liepold,[‡] Christian Griesinger,[⊥] Nils Brose,[§] Andrea Sinz,*[,∥] and Olaf Jahn*[,‡,@]

[‡]*Proteomics Group and* [§]*Department of Molecular Neurobiology, Max-Planck-Institute of Experimental Medicine, Hermann-Rein-Strasse 3, D-37075 Göttingen, Germany,* [∥]*Department of Pharmaceutical Chemistry and Bioanalytics, Institute of Pharmacy, Martin Luther University Halle-Wittenberg, Wolfgang-Langenbeck-Strasse 4, D-06120 Halle (Saale), Germany,* [⊥]*Department of NMR-Based Structural Biology, Max Planck Institute of Biophysical Chemistry, Am Fassberg 11, D-37077 Göttingen, Germany, and* [@]*Deutsche Forschungsgemeinschaft Research Center for Molecular Physiology of the Brain, Humboldtallee 23, D-37073 Göttingen, Germany*

Received February 20, 2009; Revised Manuscript Received April 29, 2009

ABSTRACT: Munc13 proteins are essential regulators of synaptic vesicle priming and play a key role in adaptive synaptic plasticity phenomena. We recently identified and characterized the Ca^{2+}-dependent interaction of Munc13 and calmodulin (CaM) as the molecular mechanism linking changes in residual Ca^{2+} concentrations to presynaptic vesicle priming and short-term plasticity. Here, we used peptidic photoprobes covering the established CaM-binding motif of Munc13 for photoaffinity labeling (PAL) of CaM, followed by structural characterization of the covalent photoadducts. Our innovative analytical workflow based on isotopically labeled CaM and mass spectrometry revealed that, in the bound state, the hydrophobic anchor residue of the CaM-binding motif in Munc13s contacts two distinct methionine residues in the C-terminal domain of CaM. To address the orientation of the peptide during binding, we obtained additional distance constraints from the mass spectrometric analysis of chemically cross-linked CaM−Munc13 peptide adducts. The constraints from both complementary cross-linking approaches were integrated into low-resolution three-dimensional structure models of the CaM−Munc13 peptide complexes. Our experimental data are best compatible with the structure of the complex formed by CaM and a CaM-binding peptide derived from neuronal NO synthase and show that Munc13−1 and ubMunc13−2 bind to CaM in an antiparallel orientation through a 1-5-8 motif. The structural information about the CaM−Munc13 peptide complexes will facilitate the design of Munc13 variants with altered CaM affinity and thereby advance the detailed functional analysis of the role of Munc13 proteins in synaptic transmission and plasticity.

Tight regulation of the cytosolic concentration of calcium ions (Ca^{2+}) is essential for the control of a wide range of biological processes, including muscle contraction, cell proliferation, apoptosis, fertilization, and neurotransmitter release. In many of these processes, an important modulatory function is carried out by CaM[1], a highly conserved intracellular Ca^{2+}-binding protein with a multitude of known interactors (*1*). Considering the extraordinarily high concentrations of CaM in the brain [10−100 μM (*2*)], it is not surprising that many of the known Ca^{2+}-dependent CaM binding partners are neuronal proteins. Because of the ability of CaM to modulate its Ca^{2+} binding characteristics in response to different target proteins, it was suggested as a candidate Ca^{2+} signal integrator in synaptic plasticity phenomena (*2*, *3*).

Prominent examples of neuronal CaM targets include the Munc13 proteins, which are the key mediators of synaptic vesicle priming, an essential process in Ca^{2+}-regulated neurotransmitter release that renders docked vesicles fusion-competent prior to exocytosis (*4*, *5*). Recently, we found that two members of the Munc13 family, Munc13-1 and ubMunc13-2, bind CaM in a Ca^{2+}-dependent manner to generate a Ca^{2+} sensor−effector complex that links residual Ca^{2+} signaling to the synaptic exocytotic machinery (*6*). The biochemical analysis of this

*To whom correspondence should be addressed. A.S.: Department of Pharmaceutical Chemistry and Bioanalytics, Institute of Pharmacy, Martin Luther University Halle-Wittenberg, Wolfgang-Langenbeck-Str. 4, D-06120 Halle (Saale), Germany; telephone, +49-345-5525170; fax, +49-345-5527026; e-mail, andrea.sinz@pharmazie.uni-halle.de. O. J.: Proteomics Group, Max-Planck-Institute of Experimental Medicine, Hermann-Rein-Str. 3, D-37075 Göttingen, Germany; telephone, +49-551-3899313; fax, +49-551-3899323; e-mail, jahn@em.mpg.de.

[1]Abbreviations: Bpa, *p*-benzoyl-Phe; BS^3, bis(sulfosuccinimidyl) suberate; BS^2G, bis(sulfosuccinimidyl)glutarate; CaM, calmodulin (L-CaM, "light" ^{14}N-CaM; H-CaM, "heavy" ^{15}N-CaM); CaMK, CaM-dependent protein kinase; DHB, 2,5-dihydroxybenzoic acid; DMSO, dimethyl sulfoxide; HCCA, α-cyano-4-hydroxycinnamic acid; HEPES, 4-(2-hydroxyethyl)-1-piperazineethanesulfonic acid; HPLC, high-performance liquid chromatography; MALDI-TOF-MS, matrix-assisted laser desorption ionization time-of-flight mass spectrometry; MLCK, myosin light chain kinase; nNOS, neuronal nitric oxide synthase; NMR, nuclear magnetic resonance; PAL, photoaffinity labeling; PDB, Protein Data Bank; SDS−PAGE, sodium dodecyl sulfate−polyacrylamide gel electrophoresis; TFA, trifluoroacetic acid.

Published on Web 05/19/2009

interaction narrowed down the CaM binding sites to a highly homologous 21-amino acid stretch in the N-termini of Munc13-1 and ubMunc13-2 (Figure 1A). These CaM binding sites are defined by a conserved bulky hydrophobic anchor residue (Trp-464 in Munc13-1 and Trp-387 in ubMunc13-2) and a high propensity to form a basic amphiphilic α-helix, minimal requirements shared by most of the otherwise rather diverse Ca^{2+}-dependent CaM binding partners (*7*). Because of the sequence diversity of its targets, CaM has to offer sufficient structural plasticity at the level of individual side chains within its target-binding interface and in the relative orientation of its domains to accommodate numerous different interaction partners. Many low- and high-resolution structural studies using both full-length proteins and shorter model peptides have provided insights into the versatile modes of interaction of CaM with its targets. Well-characterized CaM complexes include those with the smooth and skeletal muscle MLCK, CaMKII, CaMKK, and a Ca^{2+} pump (reviewed in ref (*8*)). No such structural information is yet available on the molecular recognition and activation of the Munc13 proteins by CaM, which has complicated the design of Munc13 variants with altered CaM binding characteristics. So far, we have characterized a loss-of-binding mutation (*6*), but Munc13 variants with reduced or increased affinity for CaM are expected to be more useful with regard to a detailed functional analysis of the role of Munc13 proteins in synaptic transmission and plasticity.

In a recent study, we used photoreactive Munc13-derived model peptides (termed Munc13 photoprobes) in PAL experiments to demonstrate the stoichiometric and Ca^{2+}-dependent CaM binding of Munc13 proteins (*9*). Moreover, a PAL-based Ca^{2+} titration assay revealed that Munc13 proteins can form a complex with CaM already at physiological submicromolar Ca^{2+} concentrations, underscoring the Ca^{2+} sensor−effector function of this interaction in synaptic plasticity phenomena (*9*). As PAL combined with mass spectrometry (MS) is a powerful tool for the identification of contact sites between interacting macromolecules (see refs (*10*−*12*) and recent reviews in refs (*13*) and (*14*)), we have used this methodology to provide the first structural insights into the Munc13−CaM interaction. For this purpose, we characterized the covalent complexes formed by Munc13 photoprobes and CaM at the amino acid level by applying an innovative analytical strategy based on isotopically labeled CaM and HPLC−MALDI-MS and identified a set of contact sites between Munc13 and CaM. These were complemented by a number of additional constraints revealed by chemical cross-linking and MS, another highly efficient technology for mapping protein−protein interactions in general (*15*−*18*) and CaM binding interfaces in particular (*19*−*22*). The distance constraints obtained by PAL and chemical cross-linking experiments allowed us to create low-resolution three-dimensional models of the CaM−Munc13 peptide complexes, which indicate an antiparallel alignment of the Munc13 peptides in the complex and the contribution of a 1-5-8 CaM binding motif.

EXPERIMENTAL PROCEDURES

Calmodulin. Recombinant CaM and ^{15}N-CaM were generated as described previously (*23*). Briefly, transformed *Escherichia coli* were grown in minimal medium containing NH_4Cl or $^{15}NH_4Cl$ as the nitrogen source. CaM was first enriched by a bulk purification step on the basis of TCA precipitation and further purified through hydrophobic interaction chromatography on a phenyl-Sepharose column. Collected fractions were analyzed by SDS−PAGE. Recombinant CaM was compared with bovine brain CaM in different PAL experiments as the latter was used by us in an initial PAL study with Munc13 photoprobes (*9*). No differences were found with regard to photoadduct yield, complex stoichiometry, or Ca^{2+} sensitivity (data not shown), indicating that recombinant CaM can fully replace the native protein, at least in our experimental settings. For chemical cross-linking experiments, bovine brain CaM was obtained from Calbiochem and used without further purification. By MALDI-TOF-MS, bovine brain CaM was confirmed to be N-terminally acetylated and trimethylated at Lys-115.

Photoaffinity Labeling. (i) Labeling Procedure. Photoprobes were synthesized using the photoreactive amino acid *p*-benzoyl-Phe (Bpa) as described previously (*9*, *10*). In addition to Bpa, the photoprobes also contained an artificial N-terminal Cys residue (Figure 1A) to enable a selective coupling chemistry via the sulfhydryl group, an option for future experiments that was not used in this study. For the PAL reactions, 5 μM CaM and 5 μM photoprobe were incubated for 2 h under light exclusion in 10 mM HEPES and 150 mM KCl (pH 7.2), in the presence of 30 nM free Ca^{2+} or 10 mM EGTA (see ref (*9*) for details on the Ca^{2+} buffer system). Equimolar solutions of ^{15}N-CaM were prepared in the same buffer but in the absence of photoprobe and handled in parallel. Irradiation with UV light was performed for 20 min as described previously (*9*, *10*). Subsequently, equal volumes of the PAL sample and the ^{15}N-CaM control sample were mixed. These photoreaction mixtures were analyzed by gel electrophoresis and MALDI-TOF-MS to monitor photoadduct formation and subjected to in-solution digest and HPLC−MALDI-TOF-MS to identify cross-linked peptides.

(ii) Detection of the Intact Photoadducts by Gel Electrophoresis and MS. Photoadduct formation was monitored by denaturing SDS−PAGE on precast NuPAGE 12% Bis-Tris gels (Invitrogen) using a MOPS buffer system according to the manufacturer's instructions. Proteins were visualized by colloidal Coomassie staining. MALDI-TOF-MS was used to codetect CaM, ^{15}N-CaM, and the respective photoadducts at the level of intact proteins. For this purpose, the photoreaction mixtures were desalted by RP C18 ZipTips (Millipore) and prepared according to a sinapinic acid sandwich protocol as described previously (*9*). Positively charged ions in the mass-to-charge (m/z) range of 5000−30000 were analyzed with a Bruker Ultraflex I MALDI-TOF/TOF mass spectrometer operated in the linear mode under the control of the FlexControl 2.4 operation software (Bruker Daltonik). Postprocessing of the mass spectra was performed with FlexAnalysis version 2.4 (Bruker Daltonik).

(iii) HPLC−MALDI-TOF-MS for Analysis of Photoreaction Mixtures. The photoreaction mixtures were subjected to in-solution digest with recombinant porcine trypsin (Roche) using standard conditions with the exception that 2 M urea and 10% acetonitrile were present in the digestion buffer. The resulting mixtures of tryptic peptides were separated on a Dionex Hypersil C18 BDS column (0.3 mm × 150 mm; particle size of 3 μm, pore size of 100 Å). The column was operated at a flow rate of 4 μL/min using an ABI 140B syringe pump (Applied Biosystems) connected to an Accurate splitter (Dionex). Linear gradients formed by 0.1% TFA and 0.1% TFA containing 80% acetonitrile were applied for elution. The separation was monitored by UV detection at 214 and 280 nm. Using a Probot microfraction collector (Dionex), 30 s fractions of the eluate were

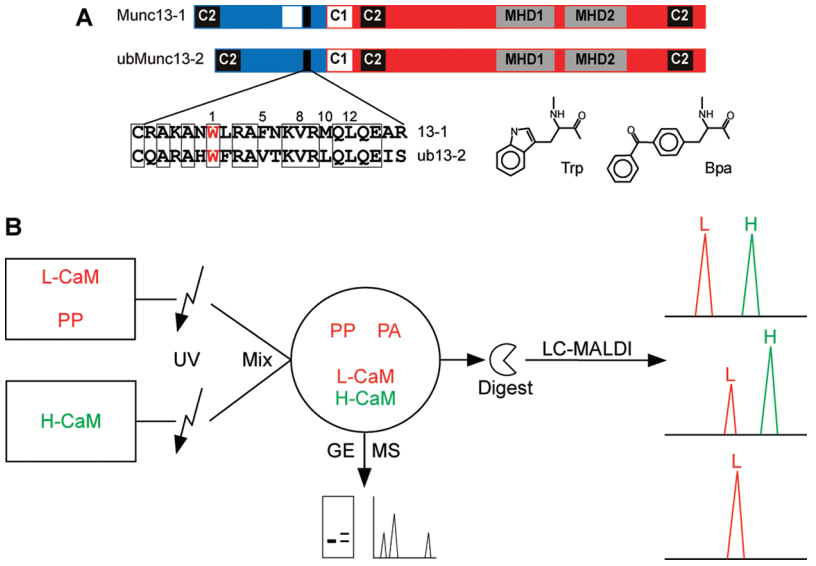

FIGURE 1: Photoaffinity labeling of CaM with Munc13-derived photoprobes. (A) Domain structure of the Munc13 proteins and photoprobe design. Munc13-1 (GenBank accession number U24070) and ubMunc13-2 (GenBank accession number AF159706) share a highly homologous C-terminus (red) with a domain structure characteristic for all Munc13 isoforms (see ref (*9*) for details). They are also related in their N-termini (blue), both containing a conserved CaM binding site [Munc13-1(459−479) and ubMunc13-2(382−402) (black rectangles)]. The sequences of the corresponding model peptides (termed 13-1 and ub13-2, respectively) are shown with identical residues boxed (59% identical). The distribution of the hydrophobic residues (starting from the anchor Trp marked in red) is indicated. In the case of the photoprobes (termed Bpa^7-13-1 and Bpa^7-ub13-2), the anchor Trp is replaced with the photoreactive amino acid Bpa, an exchange that can be considered as conservative (compare structures of Trp and Bpa). (B) Analytical strategy for mapping the sites of photoincorporation into CaM. The experimental design is based on the use of normal "light" CaM (L-CaM) as a binding partner for the photoprobe (PP) and ^{15}N-labeled "heavy" CaM (H-CaM) as a reference protein, both of which are combined after irradiation. The resulting mixture [containing L-CaM, H-CaM, the photoadduct (PA), and unreacted PP] was analyzed by gel electrophoresis (GE) and MS and finally subjected to in-solution digest followed by HPLC−MALDI-MS analysis. Three defined peak patterns were expected in the peptide survey spectra. (i) CaM fragments not involved in photoadduct formation appear as light (L) and heavy (H) doublets of similar abundance. (ii) L-CaM fragments involved in photoadduct formation are less abundant compared to their H-CaM counterparts. (iii) Unpaired light signals represent candidate cross-linked peptides (see the text for details).

automatically spotted onto a Bruker 600/384 AnchorChip target. Targets were precoated with an α-cyano-4-hydroxycinnamic acid (HCCA) matrix as described previously (*24*). To ensure uniform preparations that are independent of the eluent composition, the samples were recrystallized with a 7/2/1 tetrahydrofuran/acetone/0.1% TFA mixture (0.5 μL/spot). All peptide survey and fragment ion mass spectra were recorded on a Bruker Ultraflex I MALDI-TOF/TOF mass spectrometer as described previously (*24*). Briefly, positively charged ions in the *m*/*z* range of 500−5500 were analyzed automatically in the reflector mode under the control of the FlexControl 2.4 operation software (Bruker Daltonik). Mass spectra were automatically postprocessed with FlexAnalysis version 2.4 (Bruker Daltonik) and then manually searched for candidate cross-linked peptides. Peptides of interest were selected as precursors for the manual acquisition of fragment ion spectra, which were annotated with the help of BioTools version 3.0 (Bruker Daltonik). Relevant sample spots were subjected to on-target cyanogen bromide (CNBr) cleavage.

For comparison with observed mass spectrometric data, theoretical isotope distributions of signals corresponding to ^{14}N- and ^{15}N-containing peptides were simulated with the MS-Isotope tool of the ProteinProspector program suite (http://prospector.ucsf.edu). This tool allows simulations with variable resolution and isotope content.

(iv) On-Target CNBr Cleavage of PAL-Cross-Linked Peptides. Spot positions containing candidate cross-linked peptides were treated on-target with CNBr to directly test whether a Met side chain was involved as a site of photoincorporation into CaM (*25*). For that purpose, 2 μL of a saturated CNBr solution in 70% (v/v) formic acid was applied to the spot positions of interest. Spots were covered with small glass vials containing a filter paper soaked with the CNBr solution, and the reaction was allowed to proceed overnight at room temperature. After the reaction was terminated by evaporation of the CNBr solution, the target was directly introduced into the mass spectrometer. The corresponding peptide survey spectra were compared with those recorded before the CNBr cleavage and thereby screened for newly appearing signals corresponding to methylthiocyanate derivatives of the benzophenone-containing tryptic peptides derived from the photoprobes (monoisotopic mass shift of +73.00 mass units). The identity of such derivatives was confirmed by MS/MS sequencing.

Chemical Cross-Linking. (i) Cross-Linking Procedure. For the chemical cross-linking reactions, 10 μM CaM and 10 μM unmodified Munc13-1- or ubMunc13-2-derived peptide were incubated at room temperature in 10 mM HEPES and 150 mM KCl (pH 7.2) in the presence of 3 nM to 1 mM free Ca^{2+} (see ref (*9*) for details on the Ca^{2+} buffer system). After 1 h, reference aliquots were taken and a 50- or 100-fold molar excess of a freshly prepared DMSO solution of either BS^3-d_0/d_4 [bis(sulfosuccinimidyl)suberate, Pierce] or BS^{2}G-d_0/d_4 [bis(sulfosuccinimidyl)glutarate, Pierce] was added to the cross-linking reaction mixture. The mixture was incubated at room temperature, and aliquots were taken 5, 15, 30, and 60 min after addition of the cross-linker. For quenching the reactions, 20 mM NH_4HCO_3 was added to each aliquot, and samples were stored at −20 °C.

(ii) Linear MALDI-TOF-MS of Intact Proteins. The samples were prepared on a steel target using 1 μL of 2,5-dihydroxybenzoic acid (DHB, Sigma) matrix [50 mg/mL in 50% (v/v) acetonitrile and 0.1% (v/v) TFA] and 1 μL of a desalted

(ZipTip C4, Millipore) protein solution. MALDI-TOF-MS measurements in the linear and positive ionization mode were taken on an Ultraflex III MALDI-TOF/TOF mass spectrometer (Bruker Daltonik). Spectra in the m/z mass range of 5000−35000 were acquired under the control of FlexControl version 3.0 and processed with FlexAnalysis version 3.0 (Bruker Daltonik).

(iii) Gel Electrophoresis and In-Gel Digestion. For separation of the cross-linked species from unreacted CaM, one-dimensional SDS−PAGE (15% resolving gel) was conducted (*26*). Bands of interest were excised and subjected to in-gel digestion as described previously (*19*). Briefly, gel bands were treated with 1 μg of trypsin (sequencing grade, Roche) in 50 mM NH_4HCO_3 for 16 h at 37 °C. Peptides were extracted and stored at −20 °C for nano-HPLC−MALDI-TOF-MS analysis.

(iv) Nano-HPLC−MALDI-TOF-MS and MS/MS Analysis of Digested Cross-Linked Species. Nano-HPLC analysis of the extracted tryptic peptide mixtures was conducted with an Ultimate 3000 nano-HPLC system (Dionex). Samples were concentrated on a PepMap, RP C18 trapping column (Dionex, 5 mm × 300 μm, 5 μm, 100 Å) with 0.1% TFA at a flow rate of 30 μL/min. After 15 min, peptides were eluted onto the separation column (PepMap, RP C18, 150 mm × 75 μm, 3 μm, 100 Å), pre-equilibrated with 95% solvent A and 5% solvent B [solvent A being 5% (v/v) acetonitrile and 0.05% TFA and solvent B being 80% acetonitrile and 0.04% TFA]. Peptides were separated with the following gradient: from 0 to 30 min, 5 to 50% B; from 30 to 32 min, 50 to 100% B; from 32 to 36 min, 100% B; from 36 to 37 min, 100 to 5% B; and from 37 to 45 min, 5% B (at a flow rate of 300 nL/min). The eluates were directly fractionated by an LC/MALDI fraction collector (ProteineerFC, Bruker Daltonik) onto Bruker 800/384 AnchorChip targets (20 s/spot). Per spot, 1.1 μL of matrix [0.71 mg/mL HCCA (Sigma) in 90% acetonitrile, 0.1% TFA, and 1 mM $NH_4H_2PO_4$] was automatically added. Mass spectrometric measurements were conducted on the Ultraflex III MALDI-TOF/TOF mass spectrometer using the positive ionization and reflectron mode. Data were acquired with WarpLC version 1.1 (Bruker Daltonik) using FlexControl and FlexAnalysis scripts for data processing. For every 20 s spot, mass spectra were recorded between m/z 800 and 5000 by accumulating 1800 laser shots. For MS/MS experiments, precursor ions were selected on the basis of the characteristic isotope pattern caused by d_0 and d_4 cross-linkers (4.025 ± 0.1 amu, intensity ratios between 1/3 and 3/1, retention time tolerance of 20 s, signal-to-noise ratio of > 7).

(v) Data Analysis. GPMAW version 8.0 (Lighthouse Data) was used to compare masses of potential cross-linking products with experimental data. Candidates were verified on the basis of their MS/MS data by computing b- and y-type fragment ions by GPMAW and comparing them manually to the corresponding fragment ion mass spectra.

Computational Modeling. The structures of the Munc13 peptides were modeled using the Bhageerath program (*27*) on the basis of secondary structure predictions from JuFo (*28*) and PSIPRED (*29*). As the secondary structures of peptide N-termini were predicted to be unstructured, the first two amino acids of Munc13 peptides were eliminated before molecular docking was performed. To account for the high flexibility of CaM, structures of different CaM−peptide complexes (PDB entries 2BBM, 1CKK, 2F3Y, 1QS7, 1QTX, 2O60, 1CDL, 2FOT, and 1WRZ) exhibiting different binding modes [parallel/antiparallel; 1-10, 1-14, 1-16, IQ motifs (*30*)] were used as a starting point for fast global searches with the PatchDock server (*31*). Following earlier work (*15*, *32*), we used Lys C^{α}−Lys C^{α} distances of 5−19 Å as constraints from chemical cross-linking experiments. As the Lys side chain is highly flexible and therefore subject to conformational changes on the time scale of the cross-linking reactions, Lys C^{α}−Lys C^{α} distances, rather than Lys N^{ζ}−Lys N^{ζ} side chain distances, give a much clearer picture of the distance a cross-linker can bridge. PatchDock-created structures were used as a starting point for local searches using the RosettaDock server (*33*), in which 10000 structures were independently calculated and energetically scored. The 10 energetically best structures were filtered by the constraints obtained by PAL and chemical cross-linking, and the ones that differed less than 4 Å from the starting structures were selected. Visualization of structures was accomplished with PyMol 0.99rc6 (http://www.pymol.org/); overlay of structures was done with MultiProt [http://bioinfo3d.cs.tau.ac.il/MultiProt; (*34*)].

RESULTS

Photoprobe Design and Analytical Strategy. With the objective of identifying sites of contact between Munc13 and CaM, we generated covalent complexes of Munc13 photoprobes and CaM to be analyzed at the level of amino acids involved in cross-link formation. For this purpose, we replaced the potential anchor residue Trp-7 of the Munc13-derived model peptides 13-1 and ub13-2 (see Figure 1A for nomenclature) to generate photoprobes Bpa^7-13-1 and Bpa^7-ub13-2, respectively. Since this amino acid exchange preserves the hydrophobic, bulky, and aromatic characteristics of the anchor position (Figure 1A), binding to CaM is not impaired and Bpa^7-13-1 and Bpa^7-ub13-2 exhibit the same specific, stoichiometric, and Ca^{2+}-dependent interaction with CaM as their counterparts carrying the benzophenone moiety on the N-terminus (*9*). Moreover, previous homologous competition experiments indicated that the photoprobes and the corresponding native Munc13 peptides share the same binding site on CaM and bind with similar affinity (*9*). Taken together, by using Bpa^7-13-1 and Bpa^7-ub13-2 as photoprobes, we anticipated regioselective photoincorporation within the immediate binding cavity of CaM and thereby the direct identification of the amino acids of CaM involved in coordinating the anchor residue of the peptides.

Our innovative analytical strategy for mapping the cross-link sites in CaM is schematically shown in Figure 1B. Compared to other more common workflows, our approach omits any separation of the adduct species from unreacted CaM prior to digestion, which is usually done to prevent cross-linked peptides from being masked by an excess of unmodified CaM-derived peptides in the subsequent mass spectrometric analysis. Gel electrophoretic separation followed by in-gel digest as the most straightforward approach was only of limited use in our particular case, as the benzophenone moiety renders the cross-linked peptides highly hydrophobic and therefore hardly extractable from the gel matrix (K. Dimova and O. Jahn, unpublished observations). Moreover, reversed-phase HPLC was found to be ineffective for the purification of CaM photoadducts (*6*). To overcome these problems, we introduced a MS-based dimension of separation by using two variants of recombinant CaM: light CaM produced under standard conditions (L-CaM) and heavy CaM metabolically labeled with ^{15}N (H-CaM). Only L-CaM was employed in the PAL reaction with Bpa^7-13-1 or Bpa^7-ub13-2, while H-CaM was handled in parallel without being subjected to the reaction with the photoprobes (Figure 1B). Following irradiation, labeled

L-CaM and H-CaM were combined in an equimolar ratio, and the resulting mixture was analyzed by gel electrophoresis and MS and finally subjected to in-solution digest with trypsin (Figure 1B). Because of our experimental design with the inclusion of H-CaM as a reference protein, we expected to observe three defined peak patterns in the peptide survey spectra obtained by HPLC−MALDI-MS analysis of the tryptic digests (Figure 1B). Most of the signals should appear as characteristic doublet peaks with a fixed intensity ratio (ideally of 1/1) and a mass difference corresponding to the number of nitrogen atoms present in the respective CaM fragment. These would represent CaM sequences unaffected by the PAL reaction. The second signal species should be identical to the aforementioned doublet peaks, the exception being that the light peak shows a pronounced decrease in intensity compared to its heavy counterpart. These would represent CaM sequences directly involved in photoadduct formation. The third species should be unpaired peaks with a natural isotope distribution. These masses are not compatible with tryptic CaM peptides and therefore represent fragments of the free photoprobe (which can be sorted out easily) or cross-linked peptides, consisting of the "downregulated" CaM fragment and the Bpa-containing fragment of the photoprobe. As off-line LC−MALDI-MS circumvents the time limitations of online LC−MS couplings, these cross-linked peptides could then be subjected to extensive mass spectrometric sequencing or even to on-target manipulations such as CNBr cleavage.

Detection of Intact CaM Photoadducts and Identification of Photo-Cross-Linked Peptides. For PAL, CaM was incubated at physiological concentrations (5 μM) with equimolar amounts of photoprobe in the presence of 30 nM free Ca^{2+}, a concentration deduced as optimal from previous Ca^{2+} titration experiments (*9*). As this concentration range matches recently reported basal presynaptic Ca^{2+} levels (*35*), we feel confident that our structural results were not afflicted by artificially high Ca^{2+} concentrations. Using SDS−PAGE, Ca^{2+}-dependent complexes of CaM with Bpa^7-13-1 and Bpa^7-ub13-2 were detected as bands with an apparent molecular mass of 20 kDa (Figure 2A and Figure S1 of the Supporting Information). The high photoadduct yields of approximately 75% for both photoprobes were in agreement with previous Ca^{2+} titration experiments using bovine brain CaM (*9*).

In the following, we exemplify the in-depth analysis of the photoadducts only on the basis of the Bpa^7-13-1−CaM interaction for the sake of conciseness. We applied MS to show that the homogeneous gel bands corresponding to fractions of unreacted CaM indeed contained a mixture of L-CaM and H-CaM, differing by 177 mass units. As expected, the signals for L-CaM and H-CaM were of similar abundance when PAL was performed in the absence of Ca^{2+} (Figure 2A). Upon PAL in the presence of Ca^{2+}, the intensity of the signal for L-CaM was reduced by approximately 75%, in agreement with the photoadduct yield observed by gel electrophoresis (Figure 2A). The corresponding photoadduct of L-CaM, however, was detected at its expected m/z value, though not with the expected abundance, which probably reflects selective losses of the more hydrophobic adduct species during ZipTip desalting prior to MS.

According to our analytical strategy (Figure 1B), we next subjected the photoreaction mixture containing L-CaM, H-CaM, the photoadduct, and unreacted photoprobe to tryptic digest followed by HPLC−MALDI-MS analysis. In the peptide survey spectra obtained, most tryptic CaM fragments were detected as equiabundant doublet signals, corresponding to a CaM sequence coverage of at least 93%. These doublet signals consisted of a light peak derived from L-CaM involved in PAL and an equiabundant heavy peak derived from H-CaM included as a reference protein, as shown as an example for CaM(78−86) in panel I of Figure 2B. Consistent with the peptide sequence DTDSEEEIR containing 12 nitrogen atoms, the observed mass increment between both monoisotopic peaks was 11.98 mass units (Figure 2B, panel I). In this context, it is worth mentioning that the incorporation of ^{15}N into CaM was not complete, but 98.7% as could be determined on the basis of simulated isotope distributions (see heavy peaks in the mass spectra of Figure 2B). However, incomplete isotope incorporation turned out to be an advantage, as a signal could be readily assigned as light or heavy just on the basis of its characteristic isotope distribution without the need to know the mass distance to its respective counterpart.

When we screened the mass spectra for doublet signals with reduced intensity of the light peak compared to its heavy counterpart, we found such a peak pattern only for two CaM peptides, CaM(116−126) [light/heavy ratio of 0.75 (Figure 2B, panel II)] and CaM(127−148) [light/heavy ratio of 0.66 (Figure 2B, panel III)]. All other tryptic fragments of CaM appeared as equiabundant peak pairs, indicating that Bpa^7-13-1 exclusively labeled the CaM C-terminal domain. The corresponding cross-linked peptides consisting of one of the downregulated CaM fragments, CaM(116−126) or CaM(127−148), and the Bpa-containing photoprobe fragment, Bpa^7-13-1(5−9), were detected as unpaired peaks with a natural isotope distribution at m/z 2073.14 [$[M + H]^+_{calc,mono}$ = 2073.00 (Figure 2B, panel IV)] and m/z 3213.63 [$[M + H]^+_{calc,mono}$ = 3213.45 (Figure 2B, panel V)]. Similarly, we found characteristic peak patterns with a reduced intensity of the light peak for CaM(116−126) [light/heavy ratio of 0.88 (data not shown)] and CaM(127−148) [light/heavy ratio of 0.61 (data not shown)] when Bpa^7-ub13-2 was used for PAL. The corresponding cross-linked peptides modified by Bpa^7-ub13-2(5−9) were detected at m/z 2130.18 ($[M + H]^+_{calc,mono}$ = 2130.00) and m/z 3270.68 ($[M + H]^+_{calc,mono}$ = 3270.45) (data not shown). On the basis of the observation that the light/heavy ratio of CaM(127−148) was always lower than that of CaM(116−126), we considered the outermost C-terminus of CaM as the major and the adjacent sequence stretch as the minor contact site of Bpa^7-13-1 and Bpa^7-ub13-2. Thus, our workflow allows for a semiquantitative estimation of binding site usage. This type of information cannot be deduced from the spectral abundances of the cross-linked peptides, as these are defined by their ionization efficiencies rather than by their quantities.

Identification of Sites of Contact between Munc13 and CaM by PAL. To generate constraints that can be used for molecular modeling, we aimed at localizing the intermolecular linkage within the cross-linked peptides. We first applied MS/MS sequencing and obtained, at least for the smaller cross-linked peptide Bpa^7-13-1(5−9)−CaM(116−126), a conclusive fragment ion series, which was best compatible with a linkage of Bpa^7-13-1 (5−9) to the side chain of Met-124 (Figure 3A). In contrast, the fragment ion mass spectrum of the rather large cross-linked peptide Bpa^7-13-1(5−9)−CaM(127−148) ($[M + H]^+_{calc,mono}$ = 3213.45) did not contain instructive sequence information, but the few assignable signals again pointed to labeling of a Met present at positions 144 and 145 (data not shown). Despite the limited experimental evidence, labeling of Met residues within CaM(127−148) was considered as most likely for several reasons. First, C−H bonds adjacent to heteroatoms are known to be

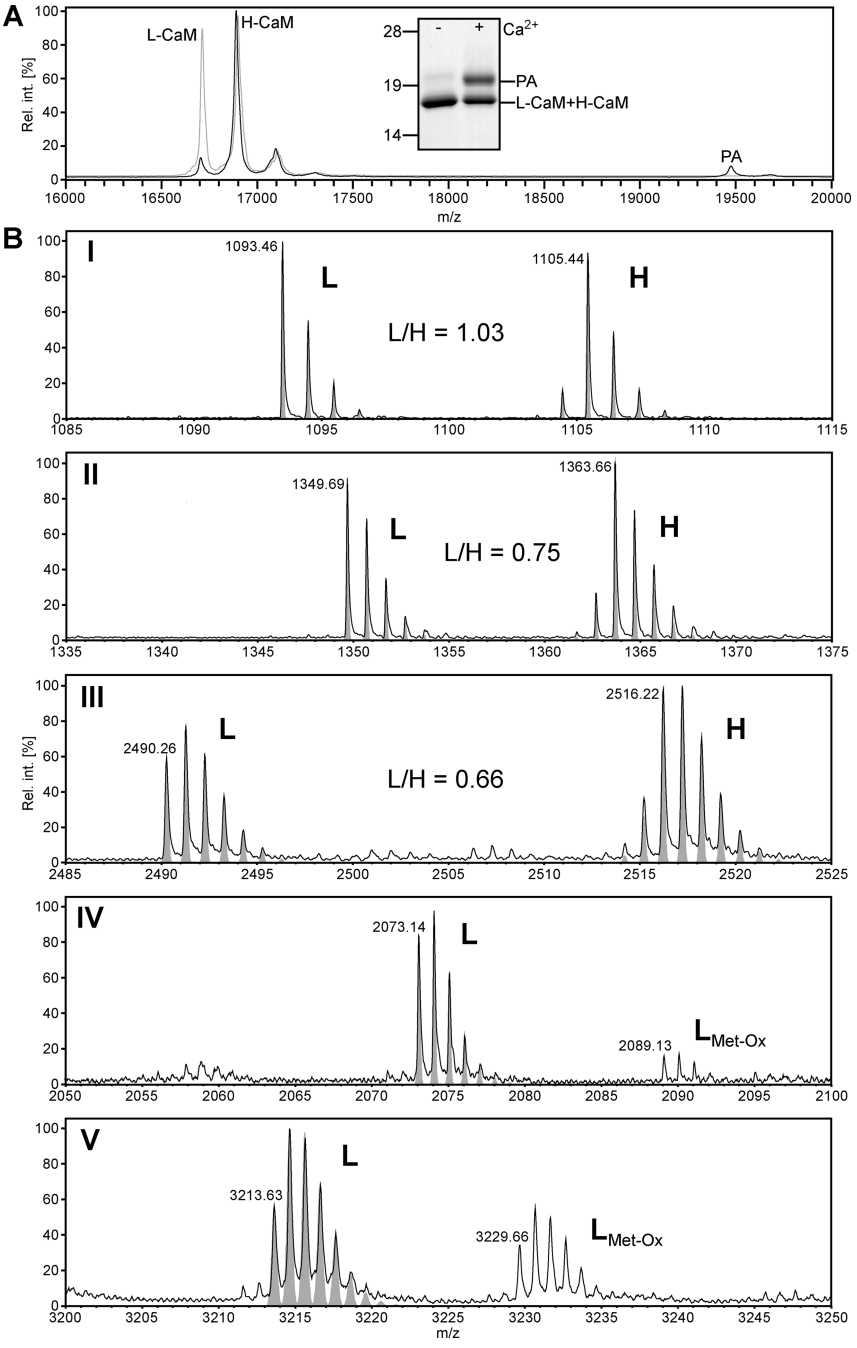

FIGURE 2: Characterization of the photoadducts at the protein and peptide level. (A) Detection of intact photoadducts by SDS−PAGE and MS. In the Coomassie-stained SDS gel (inset), the CaM photoadduct (PA) of Bpa^{7}-13-1 appeared Ca^{2+}-dependently at an apparent molecular mass of 20 kDa. Because of the experimental design (see Figure 1B), the CaM band contained L-CaM and H-CaM, which could not be distinguished by SDS−PAGE (mass difference of 177 Da). This was possible by MS as shown in the mass spectra of the same fractions (gray trace, absence of Ca^{2+}; black trace, presence of Ca^{2+}). Upon PAL in the presence of Ca^{2+}, the signals for L-CaM dropped from equiabundant levels to drastically reduced intensities compared to those of H-CaM. This was due to L-CaM's involvement in the formation of photoadduct, which was detected at its expected m/z value. For the estimation of the abundance ratio, the peak area of the H-CaM signal was corrected by approximately 25% as the sinapinic acid adduct of L-CaM (mass increment of 206 mass units) could not be distinguished from the H-CaM signal (mass increment of 177 mass units). (B) Identification of cross-linked peptides by HPLC−MALDI-MS. Selected peptide survey spectra showing characteristic peak patterns for a CaM fragment not involved in photoadduct formation [CaM(78−86), $[M + H]^{+}_{calc,mono}$ = 1093.46/1105.40 (panel I)], CaM fragments involved in photoadduct formation [CaM(116−126), $[M + H]^{+}_{calc,mono}$ = 1349.69/1363.58 (panel II), and CaM(127−148), $[M + H]^{+}_{calc,mono}$ = 2490.08/2516.00 (panel III)], and cross-linked peptides [Bpa^{7}-13-1(5−9)-CaM(116−126), $[M + H]^{+}_{calc,mono}$ = 2073.00 (panel IV), and Bpa^{7}-13-1(5−9)-CaM(127−148), $[M + H]^{+}_{calc,mono}$ = 3213.45 (panel V)]. For the CaM fragments, the light-to-heavy ratios (L/H) were calculated on the basis of the peak areas of the entire isotope clusters. Isotope distributions of the simulated peaks (shown as filled gray signals) were calculated with the MS-Isotope tool using the resolution of the corresponding observed peaks. To simulate the isotope distributions of H-CaM-related peaks, the level of incorporation of ^{15}N was set to 98.7%.

particularly reactive sites for photoincorporation of benzophenones (*36*). In the case of Met, the thioether may be involved in the formation of an intermediate radical anion/cation pair, which may account for the high reactivity of the Met side chain (*37*). Consistently, labeling of Met side chains was found in numerous PAL studies using benzophenone-derivatized peptides (see

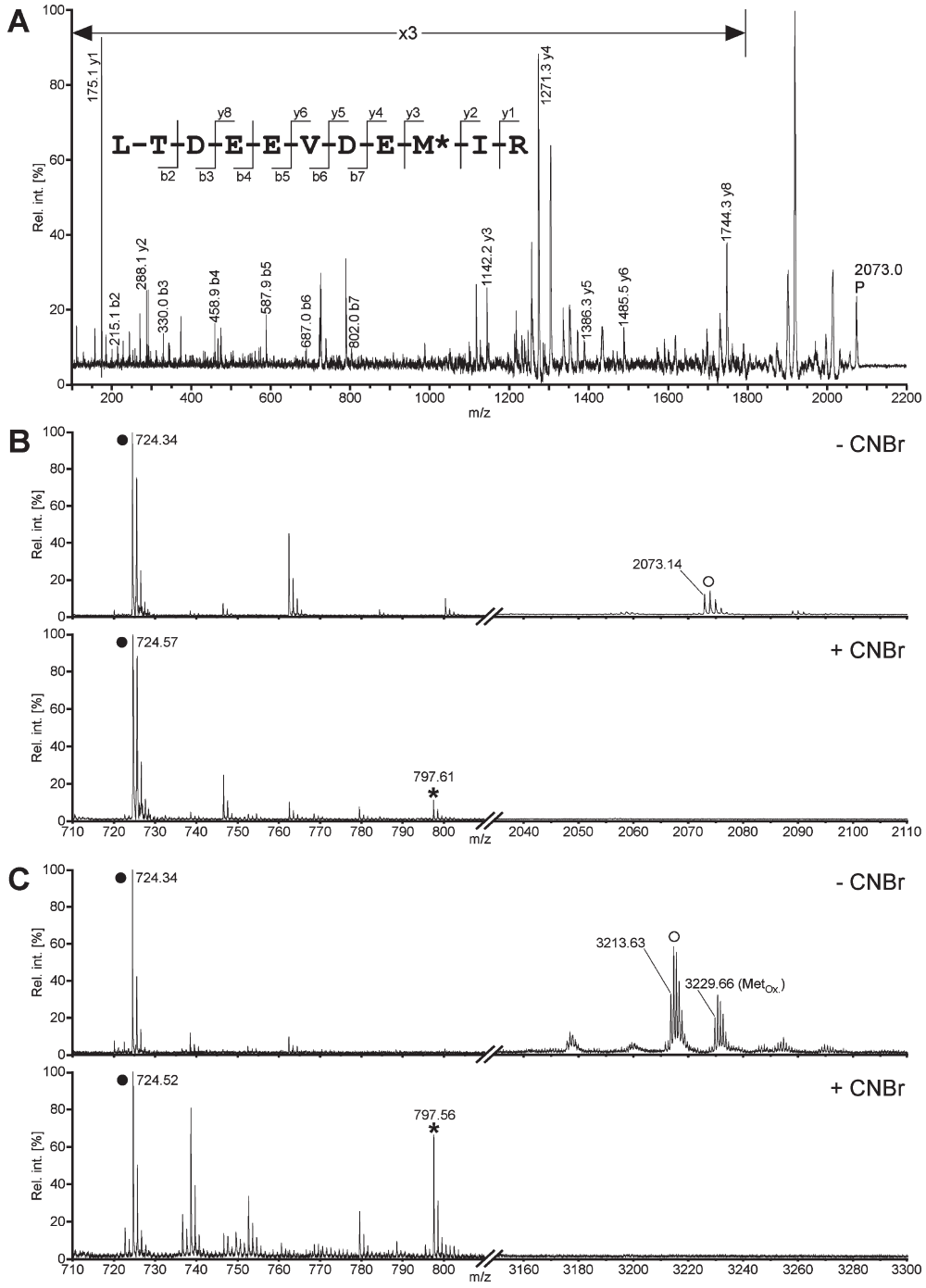

FIGURE 3: Characterization of the photoadducts at the amino acid level. (A) Fragment ion mass spectrum of the cross-linked peptide Bpa^{7}-13-1(5−9)−CaM(116−126). P denotes the precursor ion ($[M + H]^{+}_{calc,mono} = 2073.00$), and only b- and y-ions are labeled for the sake of clarity. While the N-terminal b-ion series excluded the amino acid stretch LTDEEVD as the site of modification, the y-ion series provided positive evidence that the photoprobe fragment Bpa^{7}-13-1(5−9) is linked through the side chain of Met-124 of CaM (marked with an asterisk). Note that the high abundance of the y8 ion and particularly of the y4 ion is in agreement with facile amide bond cleavages C-terminal from Asp. (B and C) On-target CNBr cleavage of the cross-linked peptides. The mass spectra were recorded from the same cross-link-containing sample spot prior to (−CNBr, top panel) and after (+CNBr, bottom panel) on-target CNBr cleavage. The middle region of the m/z range (m/z 810−2035 in panel B and m/z 810−3150 in panel C) was excluded from the x-axes to enable an appropriate display of the relevant parts of the mass spectra. Prior to cleavage, the cross-linked peptides [Bpa^{7}-13-1(5−9)−CaM(116−126) in panel B and Bpa^{7}-13-1(5−9)−CaM(127−148) in panel C (○)] were present together with the coeluting free photoprobe fragment Bpa^{7}-13-1(5−9) (●). After cleavage, the cross-linked peptide species disappeared completely, giving rise to the methylthiocyanate derivative of Bpa^{7}-13-1(5−9) (∗). The identity of this indicative CNBr product was confirmed by MS/MS sequencing (see Figure S2B of the Supporting Information).

refs (*25*) and (*37*−*40*) and references therein). Second, CaM is an extraordinarily Met-rich protein (Met frequency of 6.1%), and the Met residues constitute virtually half of its hydrophobic binding interfaces that are exposed to the solvent upon Ca^{2+} binding (*41*, *42*). Moreover, essentially all Met side chains are involved in van der Waals interactions within the high-resolution structures of CaM complexes with MLCK- and CaMKII-derived peptides (*43*−*45*). We therefore hypothesized that Met-144/145, in addition to Met-124, represents another site of contact between CaM and the anchor Trp of Munc13-1. To test this hypothesis,

we subjected the cross-link-containing sample spots to on-target CNBr cleavage. According to Kage et al. (*25*), the bond between the γ-carbon and sulfur in the Met side chain is cleaved upon treatment with CNBr, which leads to the formation of a methylthiocyanate derivative and thereby release of the benzophenone-containing photoprobe fragment. This release happens only when photoincorporation has taken place in the terminal methyl group of a Met side chain and is indicated by the appearance of a specific signal at an m/z value 73 mass units higher than that of the unmodified photoprobe fragment (*25*). As a proof of principle, we first applied this method to the cross-linked peptide Bpa^7-13-1(5−9)−CaM(116−126). Indeed, we observed that upon CNBr treatment, the cross-linked peptide dissapeared, giving rise to the methylthiocyanate derivative of Bpa^7-13-1(5−9) (see Figure 3B and the following paragraph for details). This result clearly demonstrated labeling of the side chain of Met-124 and was in full agreement with the MS/MS data (Figure 3A).

When we next subjected the larger cross-linked peptide Bpa^7-13-1(5−9)−CaM(127−148) to on-target CNBr cleavage, we observed the complete disappearance of the signals at m/z 3213.63 and 3229.66 corresponding to Bpa^7-13-1(5−9)−CaM (127−148) and its sulfoxide variant, respectively, whereas the signal at m/z 724.34 was not affected (Figure 3C). This signal corresponded to the exceptionally hydrophobic free photoprobe fragment Bpa^7-13-1(5−9) as revealed by MS/MS sequencing (Figure S2A of the Supporting Information) and was detected in several consecutive fractions at high organic modifier concentrations. More importantly, we detected a newly appearing signal at m/z 797.56 (Figure 3B) and confirmed by MS/MS sequencing that it corresponded to the methylthiocyanate derivative of Bpa^7-13-1(5−9) (Figure S2B of the Supporting Information). Thereby, labeling of CaM at Met-144/145 was demonstrated. By on-target CNBr cleavage, labeling of CaM at Met-124 and Met-144/145 was also confirmed for Bpa^7-ub13-2 (data not shown).

In summary, on-target CNBr cleavage is a straightforward method for testing whether PAL of a target protein occurred through Met, even though it is not capable of discriminating when more than one Met residue is present in the cross-linked peptide. In particular, in the case of large cross-linked peptides, on-target CNBr cleavage can complement MS/MS sequencing, which often has limitations when it comes to >3 kDa precursors. In previous PAL studies on cortocotropin-releasing factor binding protein, we successfully used endoprotease AspN in combination with trypsin for shortening the cross-linked peptides to make them available for MS/MS sequencing (*10*). However, CaM appeared to be hardly accessible for AspN. Together with the unusual abundance of potential AspN cleavage sites (17 Asp and 21 Glu residues), this led to a variety of incomplete digestion products. Thereby, the cross-link was distributed into several peptides, which often complicated or even prevented the identification of cross-linked peptides (K. Dimova and O. Jahn, unpublished observations). Moreover, incomplete cleavages often hampered the recognition of the characteristic peak patterns, which in our experimental design indicated the involvement of a particular CaM fragment in cross-link formation (see above). As AspN (or GluC) cleavage was not directly applicable, we were left with rather ambiguous MS/MS sequencing results for the large tryptic peptide Bpa^7-13-1(5−9)−CaM(127−148) (data not shown). However, we considered Met-124 and Met-144, but not Met-145, to be involved in cross-linking. The reason was that concurrent labeling of Met-124 and Met-144 was already observed in initial PAL studies on CaM using artificial model peptides with Bpa in the N-terminus of a basic amphiphilic α-helix (*38*). In these studies, modeling approaches were used to demonstrate that, depending on the orientation of the Bpa residue, labeling occurred at either Met-124 or Met-144, each of which lines opposite sides of a hydrophobic cavity in the C-terminal domain of CaM (*38*).

Detection and Separation of Chemically Cross-Linked CaM−Munc13 Peptide Adducts. Although very short and thus valuable for modeling, the few constraints from PAL were not sufficient to address the orientation of the Munc13 peptides in the complex with CaM. For this purpose, we combined our PAL approach with chemical cross-linking experiments using amine-reactive cross-linkers known to bridge Lys C^{α}−Lys C^{α} distances of up to 25 Å (*32*, *46*). Here, we employed the homobifunctional cross-linkers BS^3 and BS^{2}G, with spacer lengths of 11.4 and 7.7 Å, respectively. The cross-linking reactions were conducted with 50- and 100-fold molar excesses of cross-linker over the protein or peptide amount with reaction times ranging between 5 and 60 min. The reactions with 13-1 and ub13-2 were conducted in the presence of various free Ca^{2+} concentrations (from 3 nM to 1 mM), including 30 nM, which was found to give the highest photoadduct yield in PAL experiments (see above and ref (*9*)). Analogous to the PAL experiments, the intact cross-linking products were analyzed by MS and gel electrophoresis. Due to the relatively low yield of chemical cross-linking, the mass spectra obtained were dominated by signals related to non-cross-linked CaM, but we were able to detect peptide−protein adducts primarily of a 1/1 stoichiometry as shown for 13-1 in Figure 4A. In the presence of a 100-fold excess of BS^3, adduct yield was slightly higher than with a 50-fold excess (data not shown). Furthermore, the signal intensities for the 1/1 adducts increased with reaction time (Figure 4A), reaching plateau levels at 30 min. In the mass spectrum of the intact proteins, signals of singly [m/z 19618 for the CaM−13-1 adduct (Figure 4A); m/z 19569 for the CaM−ub13-2 adduct (data not shown)] and doubly charged ions of CaM−Munc13 peptide (1/1) adducts were detected. In addition, less intense singly charged ions were detected at higher m/z values [m/z 22558 for the CaM−13-1 adduct (Figure 4A); m/z 22528 for the CaM−ub13-2 adduct (data not shown)], indicating that both Munc13 peptides formed 1/2 adducts, at least in the presence of a 100-fold excess of BS^3. Possibly because of its higher Lys content, 13-1 has a higher propensity to form such, most likely artificial, 1/2 adducts as they were not detected for ub13-2 in the presence of a 50-fold molar excess of BS^3. Signals corresponding to protein species with a mass increased by 156, 312, and 468 mass units (i.e., 78, 156, and 234, respectively, for doubly charged ions) indicated the presence of up to two partially hydrolyzed BS^3 molecules (see the insets in Figure 4A). CaM itself was also found to be modified by up to two partially hydrolyzed cross-linkers (Figure 4A). Overall, similar reaction products were observed with BS^{2}G (data not shown).

We used gel electrophoresis to isolate the CaM−Munc13 peptide (1/1) adducts for further analysis. When Ca^{2+} concentrations in the nanomolar range (3−100 nM) were applied, bands corresponding to CaM−Munc13 peptide (1/1) adducts were detected at an apparent molecular mass of 19 kDa (Figure 4B). The maximal yields of the 1/1 adducts were estimated to be in the range of 20%. In agreement with the mass spectrometric data (Figure 4A), adduct yields increased with reaction time [most clearly up to 30 min (Figure 4B)]. At least for 13-1, also

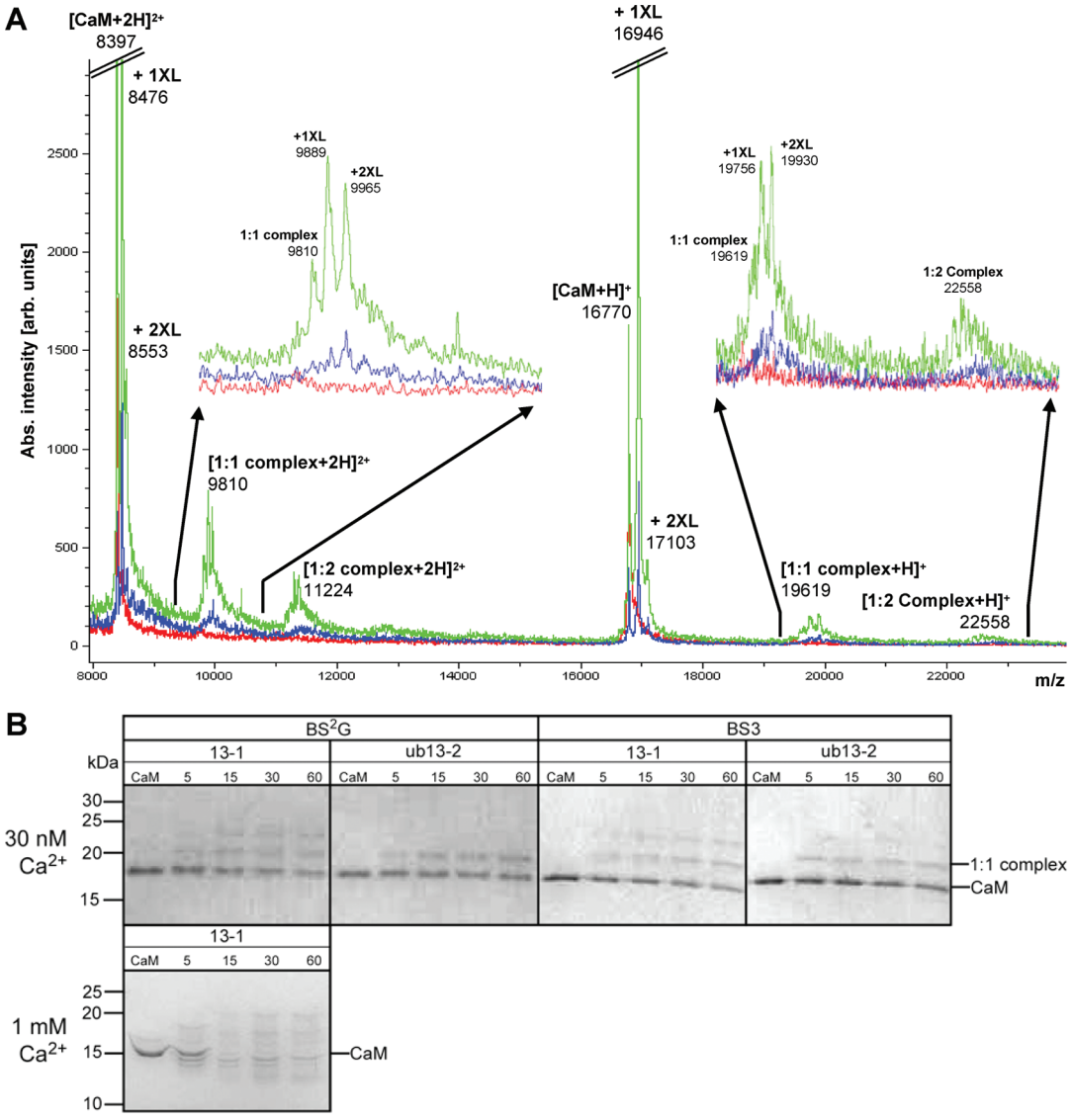

FIGURE 4: Detection and separation of chemically cross-linked CaM−Munc13 peptide adducts. (A) Mass spectra of the cross-linking reaction mixture derived from the incubation of 13-1 and CaM in the presence of 30 nM free Ca^{2+} and a 100-fold excess of BS^3. Although dominated by the signals for non-cross-linked CaM, the spectra clearly show signals for the 1/1 and 1/2 CaM−13-1 adducts, the latter having the lowest abundance. All three protein species are represented by signals of singly (right inset, *m*/*z* range of 19000−24000) and doubly (left inset, *m*/*z* range of 9400−10800) charged ions. XL corresponds to the number of bound partially hydrolyzed cross-linkers: red trace, no BS^3; blue trace, BS^3 for 15 min; green trace, BS^3 for 60 min. (B) Separation of cross-linking reaction mixtures by SDS−PAGE. A 100-fold excess of BS^3 (left column) or BS^2G (right column) was used to cross-link 13-1 or ub13-2 to CaM in the presence of 30 nM free Ca^{2+}. Time course experiments with reaction times of 5, 15, 30, and 60 min are shown. For 13-1, the same experiment under an artificially high Ca^{2+} concentration (1 mM) is shown for the sake of comparison.

well-separated CaM−peptide (1/2) adducts were observed, albeit in a lower abundance (Figure 4B). At nanomolar Ca^{2+} concentrations, adduct yields were not dependent on the type of cross-linker used; however, 13-1 formed 1/1 and 1/2 adducts with CaM faster and with higher yield in comparison to ub13-2. Interestingly, we did not detect any protein species slightly below the CaM band, which are known to be indicative of intramolecular CaM cross-linking products (*19*). In contrast, at Ca^{2+} concentrations of 1 mM, we observed smeared bands corresponding to extensive intramolecular cross-linking and heterogeneous CaM−Munc13 peptide adducts as shown for 13-1 in Figure 4B. We considered these cross-linking products as artifacts since such high free Ca^{2+} concentrations are nonphysiological in the context of the presynapse. It is likely that under such conditions the four Ca^{2+}-binding sites of CaM are presaturated prior to peptide binding, thereby preventing the stepwise Ca^{2+} loading known to be important for the cooperativity effects and conformational changes that facilitate CaM−peptide interactions (*3*, *47*).

Identification of Sites of Contact between Munc13 and CaM by Chemical Cross-Linking. To gain structural information from the cross-linking experiments, it is necessary to identify the amino acids that are actually involved in formation of the cross-link products. For this purpose, we separated the cross-linking reaction mixtures by gel electrophoresis and excised bands corresponding to CaM−Munc13 peptide (1/1) adducts. These bands were then subjected to in-gel digest by trypsin, and the resulting peptide mixtures were analyzed by nano-HPLC−MALDI-MS. Assignment of true cross-linked peptides was facilitated by the use of isotopically labeled cross-linkers as described previously (*21*). Paired peaks with the characteristic mass increment of 4 mass units were considered to represent

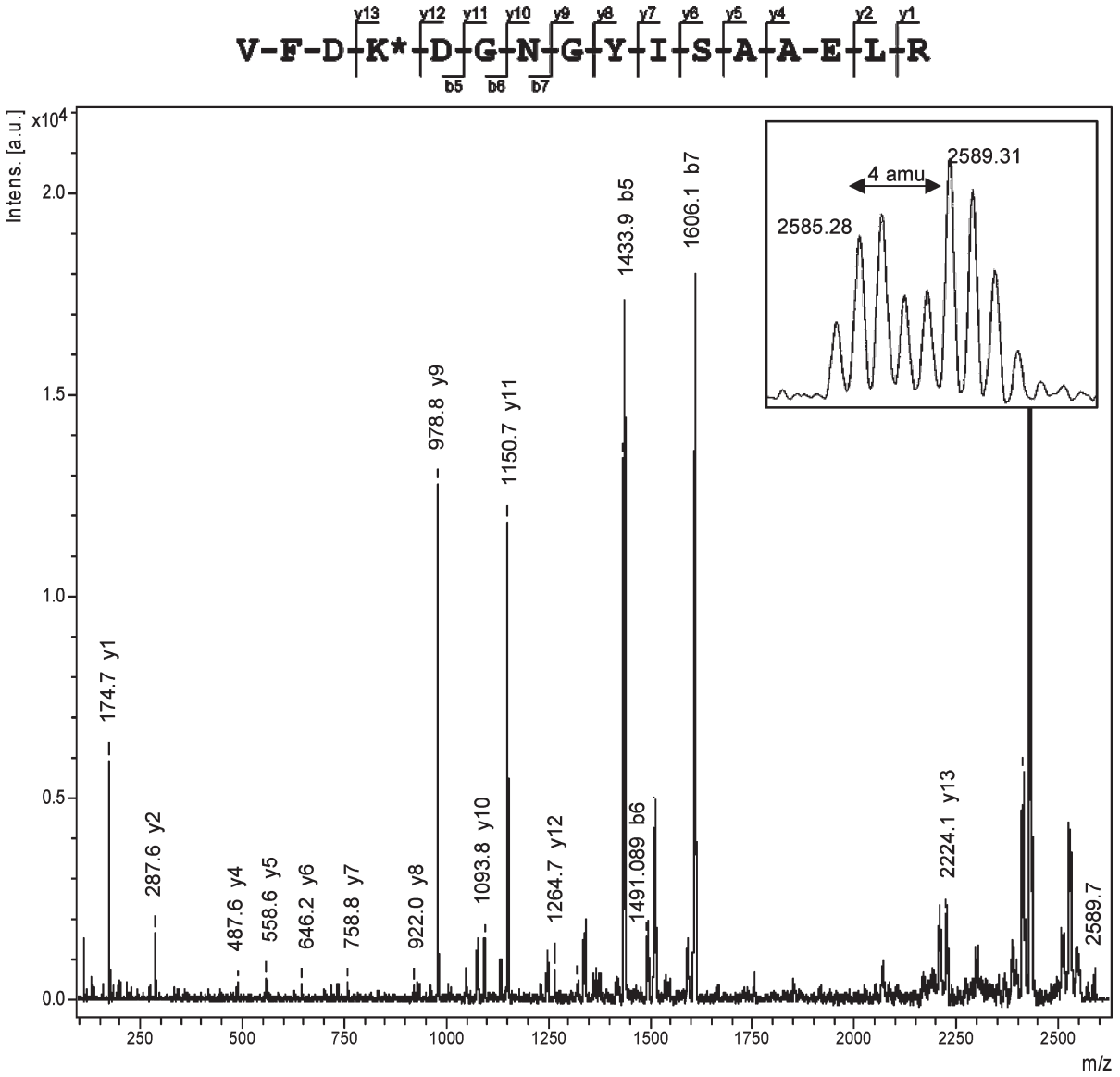

FIGURE 5: MS/MS sequencing of a cross-linked peptide. Fragment ion mass spectrum of a BS^2G-cross-linking product consisting of CaM(91−106) and 13-1(10−15). The fragment ion series y1−y13 and b5−b7 of the modified CaM peptide were detected. The mass difference between N-terminal fragment ions y12 and y13 identified Lys-94 of CaM as the cross-linked residue (∗). Moreover, the mass differences between N-terminal fragment ions y9 and y10 and C-terminal fragment ions b6 and b7 unambiguously proved deamidation of Asn-97 to Asp. The inset shows the isotope distribution of the precursor peptide as observed in the corresponding peptide survey spectrum. The characteristic signal spacing of 4 mass units is due to the concurrent application of nondeuterated BS^2G (2585.28 Da) and 4-fold deuterated BS^2G (2589.31 Da) and identifies the peptide as a true cross-linked peptide.

cross-linker-containing species. We further analyzed these pairs by MS/MS sequencing to confirm the amino acid sequences of the assigned cross-linking products, thereby identifying the cross-linked amino acids.

Analysis of the BS^3-cross-linked CaM−13-1 (1/1) adduct yielded in total seven different intermolecular cross-linking products (Table S1 of the Supporting Information), which corresponded to six contact sites (summarized in Table 1). Amino acids 10−15 of 13-1 were found to be linked to tryptic peptides derived from the N-terminal lobe (amino acids 14−30), the central α-helix (amino acids 76−86, 75−86, and 75−77), and the C-terminal lobe (amino acids 91−106) of CaM. In addition, we identified intermolecular cross-linking products, in which amino acids 14−30 and 75−77 of CaM were linked to amino acids 3−9 of 13-1. As a typical example spectrum, MS/MS sequencing of the cross-linked peptide 13-1(10−15)−CaM(91−106) is shown in Figure 5. Analysis of the BS^2G-cross-linked CaM−13-1 (1/1) adduct yielded in total six intermolecular cross-linking products (Table S1 of the Supporting Information), which corresponded to five contact sites (Table 1). Interestingly, cross-linking products containing CaM residues 91−106 were found with a mass shift of +1 mass unit compared to the calculated mass in almost all samples. The respective fragment ion mass spectra revealed that this mass shift was caused by a deamidation of CaM at Asn-97 (Figure 5).

As ub13-2 contains only one lysine residue, fewer intermolecular cross-linking products were found for the CaM−ub13-2 (1/1) adducts. BS^3 and BS^2G cross-linking yielded a large number of different products each (Table S2 of the Supporting Information), which corresponded to three contact sites (Table 1). Most of the contact sites of Lys-13 of ub13-2 were assigned to the N-terminal lobe (Lys-21) and the C-terminal lobe (Lys-94) of CaM. In summary, we identified six contact sites for Munc13-1 and

Table 1: Summary of the Sites of Contact between Munc13 Peptides and CaM As Obtained by Different Cross-Linking Techniques

		CaM											
		Lys-21	distance (Å)[a]	Lys-75	distance (Å)[a]	Lys-77	distance (Å)[a]	Lys-94	distance (Å)[a]	Met-124	distance (Å)[b]	Met-144	distance (Å)[b]
13-1	Lys-4	BS^3 BS^2G	18.9	BS^3 BS^2G	17.5	–	–	–	–	–	–	–	–
	Trp-7	–	–	–	–	–	–	–	–	Bpa	6.6	Bpa	5.0
	Lys-13	BS^3 BS^2G	17.7	BS^3 BS^2G	8.8	BS^3	12.8	BS^3 BS^2G	16.4	–	–	–	–
ub13-2	Trp-7	–	–	–	–	–	–	–	–	Bpa	7.1	Bpa	4.7
	Lys-13	BS^3 BS^2G	17.8	BS^3 BS^2G	8.9	–	–	BS^3 BS^2G	17.0	–	–	–	–

[a] Lys C^{α}−Lys C^{α} distances given for the best structures after Rosetta modeling (template CaM−nNOS peptide complex, PDB 2O60). [b] Trp $C^{\eta 2}$−Met S^{γ} distances given for the best structures after Rosetta modeling (template CaM−nNOS peptide complex, PDB 2O60).

three for ubMunc13-2, which were then used as further constraints for molecular modeling.

Creating a Model for the CaM−Munc13 Peptide Complex. On the basis of secondary structure prediction and structural modeling (see Experimental Procedures for details), it was assumed that both 13-1 and ub13-2 adopt an α-helical structure in the region comprising amino acids 4−18. Molecular docking of the α-helical Munc13 peptides to CaM was accomplished in a two-step strategy. First, fast global searches were performed using PatchDock, a program that supports the input of distance constraints (*31*). Munc13 peptides were docked to a variety of different CaM structures with simultaneous consideration of the constraints from PAL (Trp $C^{\eta 2}$−Met S^{γ} distances of 0−8 Å) and chemical cross-linking (Lys C^{α}−Lys C^{α} distances of 5−19 Å). As shown in Figure 6A, the best fit with the experimental data sets was obtained for the structure of CaM in complex with a peptide derived from neuronal NO synthase (nNOS, PDB entry 2O60). Most of the PatchDock-created structures of CaM−Munc13 peptide complexes exhibited only subtle structural differences with an overall root-mean-square deviation of < 5 Å. It is important to mention that this low variance is the result of the combination of two complementary sets of constraints derived from different cross-linking techniques. When only the constraints from PAL were applied for docking, numerous different orientations particularly of the peptide C-terminus were obtained (Figure 6B). In contrast, the overall orientation of the peptide was already quite well described on the basis of the relatively loose constraints from chemical cross-linking alone, but exact localization of the peptide N-terminus was not possible due to the lack of rather tight constraints from PAL (Figure 6C).

In the second step of the docking procedure, the structures obtained with PatchDock were refined by local searches using the RosettaDock server. When the resulting structures were filtered according to the constraints obtained by PAL and chemical cross-linking, the structure of CaM from the CaM−nNOS peptide complex was confirmed as the best-fitting structure (Figure 6D). Our modeling approach revealed that both 13-1 and ub13-2 bind to CaM as amphiphilic α-helices in an antiparallel orientation (Figure 6D and Figure S3 of the Supporting Information). In the bound state, the hydrophobic amino acids Trp-1, Phe-5, and Val-8 of 13-1 (corresponding to Trp-1, Val-5, and Val-8, respectively, of ub13-2) point toward the hydrophobic cleft of the C-terminal CaM domain, which is indicative of binding through a 1-5-8 CaM binding motif.

DISCUSSION

We present a new PAL workflow comprising the use of benzophenone photoprobes, isotopically labeled CaM, and mass spectrometry and its application in the analysis of the structure of Munc13−CaM complexes. Within our experimental strategy, we have addressed typical shortcomings of more common PAL workflows, which are often related to (i) photoprobe design, (ii) identification of the cross-linked peptides (i.e., localization of the region of photoincorporation), and (iii) sequence analysis of the cross-linked peptides (i.e., identification of the exact site of photoincorporation). First, photoprobe design is facilitated by the use of Bpa as this photoreactive amino acid can replace the hydrophobic, bulky, and aromatic anchor residues Trp and Phe that are frequently present in CaM-binding motifs, without changing the overall biophysical properties of the peptide. Moreover, benzophenones have a unique photochemistry, allowing for reversible activation even in the presence of water (*36*), and are therefore the photophores of choice when high photoadduct yields are required to obtain enough material for subsequent analysis. Second, identification of the cross-linked peptides is facilitated by the inclusion of isotopically labeled CaM (H-CaM) as a reference protein (Figures 1B and 2). Due to this experimental design, CaM sequences involved in photoadduct formation are represented by doublet peaks, the light peak of which has a reduced intensity compared to that of its heavy counterpart. Accordingly, candidate masses of corresponding cross-linked peptides can be easily derived and the mass spectra can be screened for such masses appearing as unpaired peaks with natural isotope distributions. When different CaM fragments are involved in photoadduct formation, the regulation factors of the L-CaM/H-CaM doublet peaks contain semiquantitative information of binding site usage, which cannot be derived from the mass spectrometric detection of the cross-linked peptide alone. Third, sequence analysis of the cross-linked peptides is facilitated by the use of off-line rather than on-line LC−MS techniques. Whereas the chromatographic peak width defines the analysis time in on-line couplings, LC−MALDI-MS is not limited in this respect and even enables on-target manipulations such as CNBr cleavage. We conclude that this workflow can be used in the future in the CaM field as it allows for a rapid structural screening of peptide−CaM interactions when data on the atomic structure of the complexes are lacking. Applications can also be extended to other peptide−protein interactions, at least in combination with NMR methods in which isotopically labeled proteins are often available.

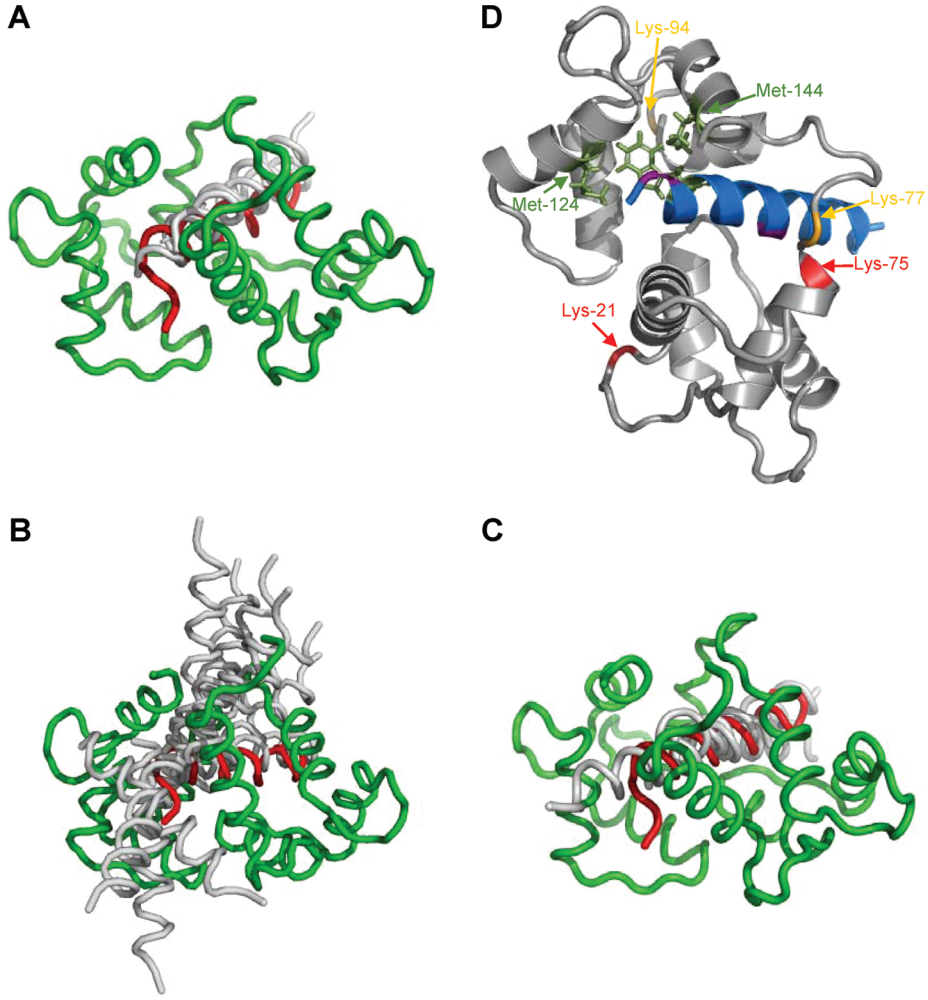

FIGURE 6: Molecular modeling of the CaM−13-1 complex. (A−C) Structures of the CaM−13-1 complex created by PatchDock on the basis of the constraints from PAL and chemical chemical cross-linking (A), PAL alone (B), and chemical cross-linking alone (C). The structure of CaM from the CaM−nNOS peptide complex (PDB entry 2O60) as the best-fitting structure is colored green. Docking solutions for 13-1 are colored gray and were limited to 10 representative structures in panel B. As shown in panel A, only two peptide structures were possible (clustering rmsd of < 5 Å) when the constraints from PAL and chemical cross-linking are combined. For the sake of comparison, the structure of the nNOS peptide (PDB entry 2O60) is colored red. (D) Model of the complex formed by 13-1 (blue) and CaM (gray) after structural refinement using the RosettaDock server. The color code of the Lys residues is as follows: yellow for CaM Lys-77/94, red for CaM Lys-21/75, and purple for 13-1 Lys-4/13. The amino acid side chains involved in PAL (Trp-7 of 13-1 and Met-124/144 of CaM) are colored green. Visualization was performed by PyMol.

Taking all lines of evidence together from the PAL experiments, we conclude that, in the bound state, the anchor residues Trp-464 of Munc13-1 and Trp-387 of ubMunc13-2 contact Met-124 and Met-144 of CaM, the latter representing the major contact site. These contacts constituted exceptionally valuable constraints for molecular modeling as they were deduced from virtually "zero-length" cross-links (see Table 1). However, PAL approaches have an inherent limitation in that they usually provide only a small number of constraints. For this reason, chemical cross-linking was applied to obtain additional constraints for model refinement and, in particular, to address the orientation of the Munc13 peptides in the bound state. Due to the complementary nature of PAL and chemical cross-linking, we were able to gain insights into both binding sites (mainly by PAL) and overall conformations (mainly by chemical cross-linking) of CaM in complex with Munc13-1 and ubMunc13-2. On the basis of the integration of all molecular distance constraints, we propose molecular models of these interactions, which, despite their low resolution, provide important structural information: CaM and the Munc13 proteins interact in an antiparallel orientation through a 1-5-8 motif. Our experimetal data are best compatible with a CaM structure similar to the one reported for its complex with neuronal NOS (PDB entry 2O60). NOS (like MLCK) contains a so-called 1-5-8-14 CaM binding motif, indicating the presence of hydrophobic anchor amino acids in positions 1, 5, 8, and 14 of the motif (*30*). Munc13-1 and ubMunc13-2 exhibit a similar CaM binding motif, with hydrophobic amino acids at positions 1, 5, 8, 10, and 12 (Figure 1A). However, the hydrophobic residue in position 14 of the CaM binding motif is missing, as is the N-terminal cluster of basic amino acids, which usually determines the orientation of the target protein in the CaM complex (*8*). We therefore conclude that Munc13 exhibits an unusual motif with a CaM binding mode similar but not identical to that of nNOS. Support for this conclusion comes from our models in which the C-terminus of 13-1 and ub13-2 differs in its conformation from that of the NOS peptide as the charged Glu residue in position 14 of the motif cannot be accommodated in the hydrophobic cleft of the N-terminal CaM domain (Figure 6A,D and Figure S3 of the Supporting Information). Because of the lack of tight PAL

constraints for the C-terminal parts of the Munc13 peptides, we cannot rule out completely the possibility that the N-terminal CaM domain adopts a more extended conformation while the peptides bind through the 1-5-8 motif to the C-terminal CaM domain as has been shown for the complex formed by CaM and C20W, a peptide derived from plasma membrane Ca^{2+} pump (*48*). However, even with more constraints available, we could hardly test this with our approach. The reason is that the CaM−C20W structure (PDB entry 1CFF) is not suitable as a template for structural docking or modeling approaches because of the inherent high flexibility of the N-terminal CaM domain leading to 26 different substructures (*48*).

On the basis of our data, we can unambiguously classify the CaM binding motif of Munc13 as a member of the antiparallel 1-5-8 motif family, even if future high-resolution structural studies are needed to elucidate the exact binding mode underlying the CaM−Munc13 interaction. Nevertheless, the combination of different cross-linking techniques, mass spectrometry, and molecular modeling is a powerful tool for complementing NMR and X-ray crystallography. In this example, our approach rapidly yielded structural information with a reasonable technical effort and, most importantly, enabled the characterization of a peptide−protein interaction under physiological solvent and concentration conditions.

Our structural data on the CaM−Munc13 complex offer new options for future studies toward a deeper understanding of the role of Munc13 in vesicle priming and short-term plasticity. Any structural information, even when of low resolution, facilitates the design of Munc13 variants with reduced or increased affinity for CaM, which are expected to be more versatile tools than the previously established loss-of-binding mutation [W464R in Munc13-1 and W387R in ubMunc13-2 (*6*)]. To generate such variants, candidate amino acid exchanges can be derived from the model structures and reintroduced into synthetic model peptides. These peptides can then be tested for CaM binding, for example, by PAL-based competition assays (*9*), and the corresponding promising mutations can ultimately be introduced into full-length Munc13 for functional studies. Although certainly challenging because of the promiscuity of CaM, a long-term aim of such future studies could even be the design of inhibitory peptides or small molecules to specifically interfere with the CaM−Munc13 interaction in vivo. Such small inhibitors would be very useful for mechanistic studies on the role of Munc13 proteins in synaptic transmission and could even be used for therapeutic purposes where inhibition of strong synaptic activity is needed (e.g., epilepsy).

ACKNOWLEDGMENT

The expert technical help of Lars van Werven in peptide synthesis is gratefully acknowledged. We also thank Lope A. Florez for his support in the initial phase of the project and Hartmut Kratzin for fruitful discussions.

SUPPORTING INFORMATION AVAILABLE

Tables S1 and S2 and Figures S1−S3 (including figure legends). This material is available free of charge via the Internet at http://pubs.acs.org.

REFERENCES

(1) Ikura, M., and Ames, J. B. (2006) Genetic polymorphism and protein conformational plasticity in the calmodulin superfamily: Two ways to promote multifunctionality. *Proc. Natl. Acad. Sci. U.S.A. 103*, 1159–1164.
(2) Xia, Z., and Storm, D. R. (2005) The role of calmodulin as a signal integrator for synaptic plasticity. *Nat. Rev. Neurosci. 6*, 267–276.
(3) Falke, J. J., Drake, S. K., Hazard, A. L., and Peersen, O. B. (1994) Molecular tuning of ion binding to calcium signaling proteins. *Q. Rev. Biophys. 27*, 219–290.
(4) Augustin, I., Rosenmund, C., Sudhof, T. C., and Brose, N. (1999) Munc13-1 is essential for fusion competence of glutamatergic synaptic vesicles. *Nature 400*, 457–461.
(5) Varoqueaux, F., Sigler, A., Rhee, J.-S., Brose, N., Enk, C., Reim, K., and Rosenmund, C. (2002) Total arrest of spontaneous and evoked synaptic transmission but normal synaptogenesis in the absence of Munc13-mediated vesicle priming. *Proc. Natl. Acad. Sci. U.S.A. 99*, 9037–9042.
(6) Junge, H. J., Rhee, J.-S., Jahn, O., Varoqueaux, F., Spiess, J., Waxham, M. N., Rosenmund, C., and Brose, N. (2004) Calmodulin and Munc13 Form a Ca^{2+} Sensor/Effector Complex that Controls Short-Term Synaptic Plasticity. *Cell 118*, 389–401.
(7) Yap, K., Kim, J., Truong, K., Sherman, M., Yuan, T., and Ikura, M. (2000) Calmodulin Target Database. *J. Struct. Funct. Genomics 1*, 8–14.
(8) Vetter, S. W., and Leclerc, E. (2003) Novel aspects of calmodulin target recognition and activation. *Eur. J. Biochem. 270*, 404–414.
(9) Dimova, K., Kawabe, H., Betz, A., Brose, N., and Jahn, O. (2006) Characterization of the Munc13-calmodulin interaction by photoaffinity labeling. *Biochim. Biophys. Acta 1763*, 1256–1265.
(10) Jahn, O., Eckart, K., Brauns, O., Tezval, H., and Spiess, J. (2002) The binding protein of corticotropin-releasing factor: Ligand-binding site and subunit structure. *Proc. Natl. Acad. Sci. U.S.A. 99*, 12055–12060.
(11) Jahn, O., Tezval, H., Spiess, J., and Eckart, K. (2003) Tandem mass spectrometric characterization of branched peptides derived from photoaffinity labeling. *Int. J. Mass Spectrom. 228*, 527–540.
(12) Jahn, O., Eckart, K., Tezval, H., and Spiess, J. (2004) Characterization of peptide-protein interactions using photoaffinity labeling and LC/MS. *Anal. Bioanal. Chem. 378*, 1031–1036.
(13) Robinette, D., Neamati, N., Tomer, K. B., and Borchers, C. H. (2006) Photoaffinity labeling combined with mass spectrometric approaches as a tool for structural proteomics. *Expert Rev. Proteomics 3*, 399–408.
(14) Vodovozova, E. (2007) Photoaffinity labeling and its application in structural biology. *Biochemistry (Moscow, Russ. Fed.) 72*, 1–20.
(15) Young, M. M., Tang, N., Hempel, J. C., Oshiro, C. M., Taylor, E. W., Kuntz, I. D., Gibson, B. W., and Dollinger, G. (2000) High throughput protein fold identification by using experimental constraints derived from intramolecular cross-links and mass spectrometry. *Proc. Natl. Acad. Sci. U.S.A. 97*, 5802–5806.
(16) Back, J. W., de Jong, L., Muijsers, A. O., and de Koster, C. G. (2003) Chemical cross-linking and mass spectrometry for protein structural modeling. *J. Mol. Biol. 331*, 303–313.
(17) Sinz, A. (2003) Chemical cross-linking and mass spectrometry for mapping three-dimensional structures of proteins and protein complexes. *J. Mass Spectrom. 38*, 1225–1237.
(18) Sinz, A. (2006) Chemical cross-linking and mass spectrometry to map three-dimensional protein structures and protein-protein interactions. *Mass Spectrom. Rev. 25*, 663–682.
(19) Schulz, D. M., Ihling, C., Clore, G. M., and Sinz, A. (2004) Mapping the topology and determination of a low-resolution three-dimensional structure of the calmodulin-melittin complex by chemical cross-linking and high-resolution FTICRMS: Direct demonstration of multiple binding modes. *Biochemistry 43*, 4703–4715.
(20) Ihling, C., Schmidt, A., Kalkhof, S., Schulz, D. M., Stingl, C., Mechtler, K., Haack, M., Beck-Sickinger, A. G., Cooper, D. M., and Sinz, A. (2006) Isotope-labeled cross-linkers and Fourier transform ion cyclotron resonance mass spectrometry for structural analysis of a protein/peptide complex. *J. Am. Soc. Mass Spectrom. 17*, 1100–1113.
(21) Schmidt, A., Kalkhof, S., Ihling, C., Cooper, D. M., and Sinz, A. (2005) Mapping protein interfaces by chemical cross-linking and Fourier transform ion cyclotron resonance mass spectrometry: Application to a calmodulin/adenylyl cyclase 8 peptide complex. *Eur. J. Mass Spectrom. 11*, 525–534.
(22) Kalkhof, S., Ihling, C., Mechtler, K., and Sinz, A. (2005) Chemical cross-linking and high-performance Fourier transform ion cyclotron resonance mass spectrometry for protein interaction analysis: Application to a calmodulin/target peptide complex. *Anal. Chem. 77*, 495–503.
(23) Haberz, P., Rodriguez-Castaneda, F., Junker, J., Becker, S., Leonov, A., and Griesinger, C. (2006) Two new chiral EDTA-based metal

chelates for weak alignment of proteins in solution. *Org. Lett. 8*, 1275–1278.
(24) Jahn, O., Hesse, D., Reinelt, M., and Kratzin, H. (2006) Technical innovations for the automated identification of gel-separated proteins by MALDI-TOF mass spectrometry. *Anal. Bioanal. Chem. 386*, 92–103.
(25) Kage, R., Leeman, S. E., Krause, J. E., Costello, C. E., and Boyd, N. D. (1996) Identification of methionine as the site of covalent attachment of a p-benzoyl-phenylalanine-containing analogue of substance P on the substance P (NK-1) receptor. *J. Biol. Chem. 271*, 25797–25800.
(26) Laemmli, U. K. (1970) Cleavage of structural proteins during the assembly of the head of bacteriophage T4. *Nature 227*, 680–685.
(27) Jayaram, B., Bhushan, K., Shenoy, S. R., Narang, P., Bose, S., Agrawal, P., Sahu, D., and Pandey, V. (2006) Bhageerath: An energy based web enabled computer software suite for limiting the search space of tertiary structures of small globular proteins. *Nucleic Acids Res. 34*, 6195–6204.
(28) Meiler, J., Muller, M., Zeidler, A., and Schmaschke, F. (2001) Generation and evaluation of dimension-reduced amino acid parameter representations by artificial neural networks. *J. Mol. Model. 7*, 360–369.
(29) McGuffin, L. J., Bryson, K., and Jones, D. T. (2000) The PSIPRED protein structure prediction server. *Bioinformatics 16*, 404–405.
(30) Rhoads, A., and Friedberg, F. (1997) Sequence motifs for calmodulin recognition. *FASEB J. 11*, 331–340.
(31) Duhovny, D., Nussinov, R., and Wolfson, H. (2002) Efficient Unbound Docking of Rigid Molecules. In Algorithms in Bioinformatics, pp 185−200, Springer, Berlin.
(32) Ye, X., O'Neil, P. K., Foster, A. N., Gajda, M. J., Kosinski, J., Kurowski, M. A., Bujnicki, J. M., Friedman, A. M., and Bailey-Kellogg, C. (2004) Probabilistic cross-link analysis and experiment planning for high-throughput elucidation of protein structure. *Protein Sci. 13*, 3298–3313.
(33) Lyskov, S., and Gray, J. J. (2008) The RosettaDock server for local protein-protein docking. *Nucleic Acids Res. 36*, W233–W238.
(34) Shatsky, M., Nussinov, R., and Wolfson, H. J. (2004) A method for simultaneous alignment of multiple protein structures. *Proteins 56*, 143–156.
(35) Lou, X., Scheuss, V., and Schneggenburger, R. (2005) Allosteric modulation of the presynaptic Ca^{2+} sensor for vesicle fusion. *Nature 435*, 497–501.
(36) Dorman, G., and Prestwich, G. D. (1994) Benzophenone Photophores in Biochemistry. *Biochemistry 33*, 5661–5673.
(37) O'Neil, K., Erickson-Viitanen, S., and DeGrado, W. (1989) Photolabeling of calmodulin with basic, amphiphilic α-helical peptides containing p-benzoylphenylalanine. *J. Biol. Chem. 264*, 14571–14578.
(38) O'Neil, K. T., and DeGrado, W. F. (1989) The interaction of calmodulin with fluorescent and photoreactive model peptides: Evidence for a short interdomain separation. *Proteins 6*, 284–293.
(39) Sachon, E., Bolbach, G., Lavielle, S., Karoyan, P., and Sagan, S. (2003) Met174 side chain is the site of photoinsertion of a substance P competitive peptide antagonist photoreactive in position 8. *FEBS Lett. 544*, 45–49.
(40) Behar, V., Bisello, A., Bitan, G., Rosenblatt, M., and Chorev, M. (2000) Photoaffinity cross-linking identifies differences in the interactions of an agonist and an antagonist with the parathyroid hormone/parathyroid hormone-related protein receptor. *J. Biol. Chem. 275*, 9–17.
(41) Peersen, O. B., Madsen, T. S., and Falke, J. J. (1997) Intermolecular tuning of calmodulin by target peptides and proteins: Differential effects on Ca^{2+} binding and implications for kinase activation. *Protein Sci. 6*, 794–807.
(42) Yamniuk, A., and Vogel, H. (2004) Calmodulin's flexibility allows for promiscuity in its interactions with target proteins and peptides. *Mol. Biotechnol. 27*, 33–57.
(43) Ikura, M., Clore, G. M., Gronenborn, A. M., Zhu, G., Klee, C. B., and Bax, A. (1992) Solution structure of a calmodulin-target peptide complex by multidimensional NMR. *Science 256*, 632–638.
(44) Meador, W. E., Means, A. R., and Quiocho, F. A. (1992) Target enzyme recognition by calmodulin: 2.4 Å structure of a calmodulin-peptide complex. *Science 257*, 1251–1255.
(45) Meador, W. E., Means, A. R., and Quiocho, F. A. (1993) Modulation of calmodulin plasticity in molecular recognition on the basis of X-ray structures. *Science 262*, 1718–1721.
(46) Green, N. S., Reisler, E., and Houk, K. N. (2001) Quantitative evaluation of the lengths of homobifunctional protein cross-linking reagents used as molecular rulers. *Protein Sci. 10*, 1293–1304.
(47) Park, H. Y., Kim, S. A., Korlach, J., Rhoades, E., Kwok, L. W., Zipfel, W. R., Waxham, M. N., Webb, W. W., and Pollack, L. (2008) Conformational changes of calmodulin upon Ca^{2+} binding studied with a microfluidic mixer. *Proc. Natl. Acad. Sci. U.S.A. 105*, 542–547.
(48) Elshorst, B., Hennig, M., Forsterling, H., Diener, A., Maurer, M., Schulte, P., Schwalbe, H., Griesinger, C., Krebs, J., Schmid, H., Vorherr, T., and Carafoli, E. (1999) NMR solution structure of a complex of calmodulin with a binding peptide of the Ca^{2+} pump. *Biochemistry 38*, 12320–12332.